journal

J. Am. Ceram. Soc., 89 [4] 1244–1256 (2006)
DOI: 10.1111/j.1551-2916.2005.00888.x

Yodel: A Yield Stress Model for Suspensions

Robert J. Flatt†

Sika Technology AG, Zürich, Switzerland

Paul Bowen

LTP, Materials Institute, EPFL, Lausanne, Switzerland

A model for the yield stress of particulate suspensions is presented that incorporates microstructural parameters taking into account volume fraction of solids, particle size, particle size distribution, maximum packing, percolation threshold, and interparticle forces. The model relates the interparticle forces between particles of dissimilar size and the statistical distribution of particle pairs expected for measured or log-normal size distributions. The model is tested on published data of sub-micron ceramic suspensions and represents the measured data very well, over a wide range of volume fractions of solids. The model shows the variation of the yield stress of particulate suspensions to be inversely proportional to the particle diameter. Not all the parameters in the model could be directly evaluated; thus, two were used as adjustable variables: the maximum packing fraction and the minimum interparticle separation distance. The values for these two adjustable variables provided by the model are in good agreement with separate determinations of these parameters. This indicates that the model and the approximations used in its derivation capture the main parameters that influence the yield stress of particulate suspensions and should help us to better predict changes in the rheological properties of complex suspensions. The model predicts the variation of the yield stress of particulate suspensions to be inversely proportional to the particle diameter, but the experimental results do not show a clear dependence on diameter. This result is consistent with previous evaluations, which have shown significant variations in this dependence, and the reasons behind the yield stress dependence on particle size are discussed in the context of the radius of curvature of particles at contact.

I. Introduction

The rheological behavior of concentrated particle suspensions plays an important role in many industrial processes such as ceramic slurry processing (slip casting, tape casting, filter pressing), paints, cement and concrete placement, cosmetics, and pharmaceutical formulations. The interparticle forces that arise from dispersion forces, electrostatic interactions between charged surfaces, and the steric forces from adsorbed polymers all have to be taken into account when trying to understand and predict the rheological properties. When suspensions have a very high volume fraction of solids and are put into movement by shear forces, hydrodynamic interactions and crowding also play important roles. When the overall interaction potential is attractive, there is a certain volume fraction of solids whereby a continuous network is formed and a certain shear stress is needed to overcome the interparticle forces to induce flow. This shear stress or yield stress has been shown by many studies to be dependent on the interparticle forces, the volume fraction, particle size, and size distribution.[1–4] Attempts to predict and model the rheological behavior of suspensions as a function of particle size, interaction energy, and volume fraction of solids have received considerable attention. The shear yield stress often follows a power-law function with respect to the volume fraction of solids,[5] and although models to link this to the microstructure are beginning to achieve some success for low volume fractions of solids,[6] further work on linking microstructure to flow properties is needed.

The prediction of rheological properties with respect to interparticle forces has in general shown very good qualitative agreement but has not yet shown quantitative agreement.[7,8] One of the reasons often stated for the poor agreement is that all the interparticle interactions are a function of particle size and size distribution—most calculations being limited to using some type of median or average diameter, i.e., oversimplifying the microstructural contribution. Strauss *et al.*[9] demonstrated many years ago the effect that a particle size distribution should have on the interparticle interactions and dispersion stability. Therefore, for materials such as cement, which have broad size distributions, taking into account the size distribution and its microstructural consequences should be important. Zhou *et al.*[4] found for several alumina powders and mixtures of these powders that the experimentally measured yield stress scaled on the surface and not the number or volume average diameter. However, the reason why this should be so was not entirely resolved, once more demonstrating the need for a better understanding of the microstructural contribution.

The development of the model presented in this paper was motivated by the desire to predict the rheological behavior of cementitious systems. In particular, we are interested in relating the properties of adsorbed dispersants, superplasticizers, to macroscopic flow behavior. The dispersion of cement is a crucial step in obtaining a highly flowable concrete with minimum water content, so that the ultimate hardened material will show improved strength and durability.[10,11] The general role of admixtures has already been discussed in some detail elsewhere.[12] Although the model is specifically aimed at cementitious systems, it is also of great relevance for casting techniques such as gel casting and coagulation casting, where high solids loading with low viscosity is needed.[13] Filling molds of complicated shapes with the highest solids loadings possible are essential for the success of these techniques. The model will help researchers compare the relative effects of PSD, steric, and electrostatic interactions for a maximum volume fraction of solids. This will allow green bodies with high homogeneity and low shrinkage with near net shape to be formed—a key issue when green machining is either too difficult or too expensive. Also, for tape casting in aqueous media, the need for better control or prediction of the yield stress would help in the formulation and help us close the gap with the environmentally less acceptable non-aqueous approaches.

In the present article, we focus on the dependence of yield stress on the volume fraction of solids. For this, we resort to

G. Franks—contributing editor

Manuscript No. 20859. Received August 9, 2005; approved November 11, 2005.
†Author to whom correspondence should be addressed. e-mail: flatt.robert@ch.sika.com

better defined systems, for which the necessary data are available in the literature. The model that we propose accounts for particle size distribution, mean particle size, volume fraction of solids, maximum packing fraction, percolation threshold, and interparticle forces. This model introduces more microstructural information, but some pragmatic choices of certain parameter values are needed in its derivation. Nevertheless, their magnitudes are physically coherent and in agreement with independent evaluations.

II. Background

(1) Interparticle Forces

In this paper, particles can either be considered as spheres or as particles that have spherical curvatures at interparticle contact points.[13–15] In the range of small separations, it can be shown that the forces between two spherical particles are all proportional to the harmonic average of the radii $\bar{a} = 2a_1a_2/(a_1 + a_2)$ of the two particles of radius a_1 and a_2. For particles that are not spherical, but for which contact points have roughly spherical curvatures, the forces would scale with a mean radius of curvature, which we denote as a^*. For generality of the treatment, we will use the notation $\tilde{a}$ for both cases.

For the van der Waals force, we have[14]

$$F_{\mathrm{VDW}} \cong \frac{1}{12} A_{(\mathrm{h})} \left(\frac{\tilde{a}}{h^2}\right) \tag{1}$$

where $A_{(\mathrm{h})}$ is the retarded Hamaker constant (related to the dielectric properties of the material and the medium) and h is the separation distance between particles. Values of Hamaker constants at zero separation are given by Bergström,[15] while expressions for retardation can be found elsewhere.[14,16]

For electrostatic forces, in the range of low potentials, we have[16,17]

$$F_{\mathrm{ES}} \cong -2\pi\varepsilon\varepsilon_0\tilde{a}\psi^2 \frac{\kappa e^{-\kappa(h-2L_e)}}{(1 + e^{-\kappa(h-2L_e)})} \tag{2}$$

where ε_0 is the permittivity of vacuum, ψ is the electrostatic potential, ε is the relative dielectric constant of the continuous phase, κ^{-1} is the Debye length given by $\sqrt{\varepsilon\varepsilon_0 k_B T/2e^2 z_{eq}^2 n_{eq}^b}$, z_{eq} is the valence of the (equivalent) electrolyte, n_{eq}^b is the bulk concentration of the symmetric (equivalent) electrolyte, and L_e is the distance from the particle surface used as the plane of origin for the electrostatic repulsion. This is often taken as the particle surface, but for charge induced by certain superplasticizers (polyelectrolytes), it may be closer to the polymer–liquid interface rather than the particle surface.

In the case of adsorbed dispersants, the steric force depends on the assumed conformation and surface coverage. For two interacting spheres and adsorbed polymer where the end-grafted chains assume a mushroom conformation, the de Gennes model[18] along with the Derjaguin approximation leads to

$$F_{\mathrm{Ster}} = \tilde{a}\frac{3\pi k_B T}{5s^2}\left[\left(\frac{2L_S}{h}\right)^{5/3} - 1\right] \tag{3}$$

where s is the distance between the centers of gravity of two neighboring mushrooms. L_S is the maximum length extending into the solvent.

The total interaction force can be obtained by taking the sum of Eqs. (1)–(3). As all these equations depend linearly on $\tilde{a}$, it is possible to introduce an interparticle force parameter $G_{(\mathrm{h})}$ given by

$$G_{(\mathrm{h})} \cong \frac{F_{\mathrm{VDW}} + F_{\mathrm{ES}} + F_{\mathrm{Ster}}}{\tilde{a}} \tag{4}$$

We note that when an admixture induces little surface charge on adsorption and is present in sufficient amount at the surface (e.g., a polyacrylate superplasticizer), there is little interpenetration and the maximum force occurs essentially for a separation distance equal to twice the adsorbed layer thickness. A similar situation would be that of some hydration layer that would not contribute to van der Waals forces. In these cases and neglecting retardation, an estimation of this minimum separation distance, H, allows us to determine the maximum value of the interparticle force parameter $G_{\max}$ as

$$G_{\max} \cong \frac{A_0}{12H^2} \tag{5}$$

(2) Rheology of Alumina Suspensions

The Melbourne group has conducted extensive studies on the rheology of various metal oxide suspensions.[19–21] Of relevance to this paper is their study of the role of particle size, volume fraction of solids, and pH on shear yield stress; the results were obtained using the vane technique.[22,23] They showed clearly, as expected, that yield stress increases with increasing volume fraction of solids and with decreasing particle size. Another expected result is that the yield stress has a maximum at the isoelectric point (IEP). This results from the absence of electrostatic repulsion. Above and below this pH, the particles are charged and yield stress is lower.[21]

In a first attempt to rationalize these data, Kapur *et al.*[2] proposed an extension of Rumpf's treatment of the tensile strength of a bed of monosized particles[24] in order to account for polydispersity. In summary, Rumpf's model equates the tensile strength of a bed of particles to the product of a number of particle contacts per unit area and the force linking the said particles. Kapur's model essentially does the same for shear yield stress using analytical expressions for the coordination number in a size-distributed system.[25] As a result, the two models have similar limitations, which arise both from an idealization of microstructure and from overlooking the role of flaws. Another issue that does not seem to have been discussed sufficiently is the step from a model aimed at predicting tensile strength to a model aimed at describing shear yield stress. Indeed, for tensile strength, on the one hand, one might expect a monotonous increase with volume fraction until the maximum packing is reached. On the other hand, for yield stress (assumed to characterize a solid to liquid transition), one tends to observe a divergence as the maximum packing is approached. From this, one might expect that the Kapur model does not necessarily capture the correct dependence of yield stress on the volume fraction of solids. Indeed, in the paper of Kapur *et al.*, an additional dependence on the volume fraction of solids was introduced for the minimum interparticle separation distance H in the form of

$$H = h_0(9.5\exp(-4.5\phi)) \tag{6}$$

Essentially, this implies that the interparticle force is dependent on the volume fraction of solids in suspension.

In a later paper dealing with alumina suspensions, Zhou *et al.*[19] presented results that, on the contrary, indicated that interparticle forces were not volume fraction dependent. This conclusion was reached by a series of data normalizations that are best described in a later review of this work.[21] The data analysis they conducted started with a data series of shear yield stresses measured as a function of pH. Each data series (given powder and varying volume fraction of solids or a given volume fraction of solids and different powders) showed a maximum yield stress $\tau_{\max}$, the yield stress at the IEP followed by a decrease more or less symmetrically at a higher and lower pH. The authors found that normalizing each data series by its value of $\tau_{\max}$ collapsed all data onto a master curve that no longer showed a dependence on volume fraction of solids or particle size.[21]

There is a very important implication to this result. It is that all the microstructural information built into the yield stress of

these systems can be decoupled from interparticle forces. Thus, the study of yield stress at the IEP should yield the microstructural information, while studies over a range of pH should yield the dependence on interparticle forces.

To examine the latter issue, Zhou *et al.* considered that the interparticle force was the result of a van der Waals attraction and a repulsive electrostatic force. Furthermore, they considered that the particles would have a well-defined non-zero separation distance when they are in contact. Under these conditions, simplified expressions of the interparticle forces predict that the normalized yield stress should decrease linearly with the square of zeta potential ζ according to

$$\frac{\tau_y}{\tau_{max}} = 1 - \frac{24\pi\varepsilon\varepsilon_0\kappa H^2}{A_0(1+e^{\kappa H})}\varsigma^2 \quad (7)$$

where H is the non-zero minimum separation distance that the particles are assumed to adopt upon contact.

We note that these results come from the ratio of $F_{VDW}+F_{ES}$ over F_{VDW} and that particle size dependence disappears. Thus, the relation between the normalized yield stress and the square of zeta potential can be expected to be rather independent of particle shape, while the slope will depend on particle shape. Furthermore, under the condition of spherical curvatures at contact points, the same result is obtained.

Zhou *et al.* did indeed find their plots of normalized yield stress versus the square of zeta potential to be linear. Furthermore, they used the slope from such plots along with (7) to determine the value of H. These are found to be quite similar for the different-sized alumina powders, as shown in Table I, and the average is about 2.4 nm.

The remaining issue is to predict yield stress at the IEP. Kapur's model predicts that it should vary with the inverse of the particle size,[2] as the interparticle force varies linearly with particle size, while the number of contacts varies with the inverse second power of particle size.[16] However, the analysis of Zhou *et al.* suggests that yield stress scales with the inverse second power of the particle size. They indicate that they do not have a physically based explanation for the scaling that they obtain with particle size, and suggest it may have arisen from the non-sphericity or from microstructural effects. In a later paper, they suggest that the average coordination number should depend inversely on particle size.[21] In determining the nature of this particle size dependence, various average particle sizes were considered. The one that appeared to give the most consistent results was based on a surface average diameter. This was supported by the fact that in bi-, tri- and tetramodal suspensions, the surface average diameter of the components led to a good prediction of yield stress as a function of the proportion of the various solids in suspension.[19]

In this paper, we present a derivation of a model for yield stress that is based on first principles. It leads to a different dependence of volume fraction, introducing a divergence at the maximum packing fraction of solids as well as a percolation threshold. This model fits extremely well the shear yield stress of the four alumina powders with narrow size distributions used by Zhou *et al.* Furthermore, this result is obtained with the same percolation threshold and maximum packing values and holds throughout the entire range of volume fractions (in contrast to Zhou *et al.,* who propose two distinct fitted power laws to cover the entire range of volume fractions). When this new volume fraction function is used to analyze these data, the same inverse second power dependence on particle size is obtained, which we attribute to a characteristic radius of curvature at particle contacts, a^*, that does not scale with particle size.

Table I. Inferred Separation Between Alumina Particles in Contact[19]

Sample	AKP-15	AKP-20	AKP-30	AKP-50
H (nm)	2.6	2.4	2.3	2.6

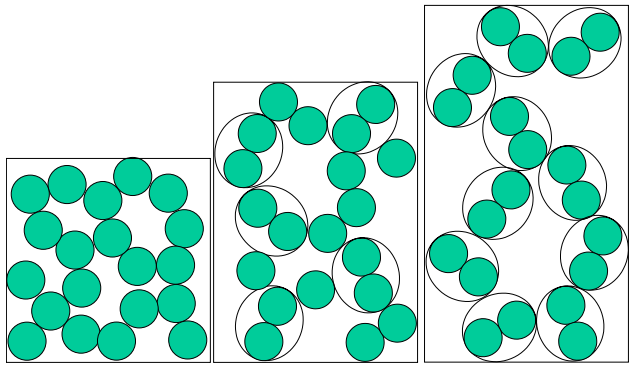

Fig. 1. Schematic representation of the change in effective volume or maximum packing as a function of the increase in the number of unbroken bonds. These unbroken bonds can be considered to either increase the effective volume of solids or decrease the maximum packing. As discussed below, both situations are equivalent.

III. Derivation of the Yield Stress Model (YODEL)

(1) General Principle

The basic idea behind the YODEL is to identify the number of particles in contact with each other and that cannot be separated from one another by the applied shear stress. It is these unbroken interparticle bonds that are responsible for yield stress of the suspension. Our aim is to express this relation in quantitative terms.

Figure 1 illustrates three cases for spheres where an increasing number of interparticle bonds cannot be broken by the applied shear force. We consider that each pair of particles behaves as a new individual particle with a larger effective volume than the sum of the two individual particles it is made of.

At this stage, the exact choice of the magnitude of this volume increase is of only secondary importance as we only wish to illustrate the principle. What is more important is that we consider that an increase in the number of unbroken bonds increases the volume needed to pack a given number of primary particles and that this will be associated with an increase in yield stress. Overall, the way in which we formulate this and develop our model may be viewed in two separate but mathematically equivalent ways. These are as follows:

In the first situation, we consider that each unbroken bond increases the volume fraction ϕ of the solid phase to an effective volume fraction denoted ϕ^*. The increment of the effective volume fraction of the solid phase will depend on the applied shear τ, interparticle force parameter G, solid content, and hence the particle size distribution. It can be noted as $\Delta\phi(G,\tau,\phi)$.

The suspension is considered to yield when the effective volume fraction of the solid phase, given by $\phi^* = \phi + \Delta\phi(G,\tau_0,\phi)$, is equal to the absolute maximum packing fraction of the powder ϕ_{max}. The packing fraction is a constant that only depends on the shape and size distribution of the powder.

The yield condition outlined above may thus be equated as

$$\Delta\phi(G,\tau_0,\phi) = \phi_{max} - \phi \quad (8)$$

The other way of viewing the problem is by considering that each unbroken bond reduces the maximum packing of the powder to an accessible maximum packing fraction ϕ^*_{max}. This means that this maximum packing fraction now takes into account agglomerates and the pore volume included. It is an experimental maximum packing for a specified applied shear. In Fig. 1, each box contains the same number of primary particles, and hence the solid phase in the suspension remains constant, but the maximum packing decreases from left to right. The dif-

ference between the accessible maximum packing, ϕ^*_{max}, and real maximum packing, ϕ^*, also depends on the applied shear, interparticle force parameter, volume fraction of solids, and particle size distribution. We can write it as $\Delta\phi_{max}(G, \tau, \phi)$.

In a similar way as before, we consider that the suspension yields when the true volume fraction ϕ of the solid phase is equal to the accessible maximum packing, which may be written as $(\phi^*_{max} = \phi_{max} - \Delta\phi_{max}(G, \tau_0, \phi))$. In other words, our yield condition becomes

$$\Delta\phi_{max}(G, \tau_0, \phi) = \phi_{max} - \phi \tag{9}$$

Provided we use the same expression for $\Delta\phi(G, \tau, \phi)$and $\Delta\phi_{max}(G, \tau, \phi)$, both situations lead to the same result. In what follows, we will just use $\Delta\phi$ to refer either to $\Delta\phi(G, \tau, \phi)$ or $\Delta\phi_{max}(G, \tau, \phi)$.

The most delicate aspect of this model is obtaining a credible expression for $\Delta\phi$ with as much sound physical meaning as possible.

A point of detail concerning Fig. 1 is that as outlined below, the force balance that we used to determine whether an applied shear stress can separate particles leads to a result that depends on the initial orientation assumed. We have dealt with this issue by determining the fraction of orientations that will not allow particles to be separated. In doing so, we introduce a subsistence probability, which results in removing the existence of a unique shear value below which all particles are stuck together and above which they all separate. Thus, the situations considered in the center and right illustration of Fig. 1, where not all particles are linked together, are consistent with our treatment.

(2) Doublet Subsistence Probability

(A) Force Balance: Let us consider a doublet of random orientation composed of two spherical particles S_k and S_l, as represented in Fig. 2(a). The interparticle force, F, between this pair is represented in Fig. 5(b). Its components are

$$\begin{aligned} F_x &= F \sin\theta \cos\varphi \\ F_y &= F \sin\theta \sin\varphi \\ F_z &= F \cos\theta \end{aligned} \tag{10}$$

The shear force is applied in the x-direction. Thus, depending on the orientation of the doublet, this may or may not exceed the projected interparticle force in that direction. If it does, separation may begin. Otherwise, doublets will subsist and contribute to the yield stress (or higher viscosity). We will determine the subsistence probability as the fraction of configurations that can be separated at a given shear stress. In reality, we only do this for the configurations that have the potential of being separated, neglecting the situation where the applied shear pushes the particles together. We assume that any such doublet might undergo a 90° rotation and might also undergo separation.

(B) Stress for Doublet Separation: Let us consider a suspension below its yield point in a regime that may be described as that of a solid. For a randomly oriented doublet, the shear stress, which can effectively be used to separate the doublet, is given by

$$\tau_{k,l,\theta} = \tau_{k,l} \cos\theta \tag{11}$$

This indicates that the stress is equal to zero if the doublet is aligned in the direction in which stress is applied, while it is maximum if the doublet is perpendicular to this direction. This can be equated to the x-axis projection of the interparticle force, normalized by the average surface $\bar{\Omega}_{k,l}$, over which the stress is applied:

$$\tau_{k,l} \cos\theta = \frac{F \sin\theta \cos\varphi}{\bar{\Omega}_{k,l}} \tag{12}$$

Replacing the force by the maximum attractive interparticle force ($F_{max} = G_{max}\tilde{a}$) and using Eqs. (11) and (12), we obtain the ratio of the maximum interparticle force with the shear stress per doublet:

$$\frac{G_{max}}{\tau_{k,l}} = \frac{\bar{\Omega}_{k,l}(\cos\theta/\sin\theta)(1/\cos\varphi)}{\tilde{a}} \tag{13}$$

We now need to determine the average surface over which the shear stress must be applied per individual doublet. For this, we choose to first calculate the average intersection surface of a shear plane with each sphere:

$$\bar{\Omega}_i = \frac{\int_{-a_i}^{a_i} \pi(a_i^2 - h^2)\, dh}{\int_{-a_i}^{a_i} dh} = \frac{\pi}{2a_i}\left(2a_i^3 - \frac{2a_i^3}{3}\right) = \frac{2}{3}\pi a_i^2 \tag{14}$$

Then, we take the average of $\bar{\Omega}_k$ and $\bar{\Omega}_l$ of both these surfaces to determine $\bar{\Omega}_{k,l}$:

$$\bar{\Omega}_{k,l} = \frac{\bar{\Omega}_k + \bar{\Omega}_l}{2} = \frac{\pi}{3}\left(a_k^2 + a_l^2\right) \tag{15}$$

Substituting Eqs. (14), (15) into Eq. (13), we obtain

$$\frac{G_{max}}{\tau_{k,l}} = \frac{\pi\left(a_k^2 + a_l^2\right)}{3\tilde{a}} \frac{\cos\theta}{\sin\theta} \frac{1}{\cos\varphi} \tag{16}$$

which expresses the fact that the stress per doublet that must be applied to separate the given doublet not only depends on the maximum interparticle force but also on the initial orientation.

For convenience, we normalize all radii a by the median volume radius $R_{v,50}$ and denote them as b.

$$\frac{G_{max}}{\tau_{k,l} R_{v,50}} = \frac{\pi\left(b_k^2 + b_l^2\right)}{3\tilde{b}} \frac{\cos\theta}{\sin\theta} \frac{1}{\cos\varphi} \tag{17}$$

(C) Stress Transmission Through a Network: Below the yield point, and at slow deformations, stress is transmitted only through the percolating network, so that the stress per doublet is linked to the stress applied to the suspension. Assume that we fix the value of G/τ, where τ, here, is the shear stress applied to the suspension. It is related to the shear stress a given doublet undergoes by

$$\tau_{k,l} = \frac{\tau}{\phi - \phi_0} \tag{18}$$

where ϕ_0 is the percolation threshold.

Thus, at a given stress applied to the suspension, the stress per bond decreases with increasing volume fraction of the solid phase.

We emphasize that this holds for yield stress defined as the initiation of flow from the breakdown of a percolating network.

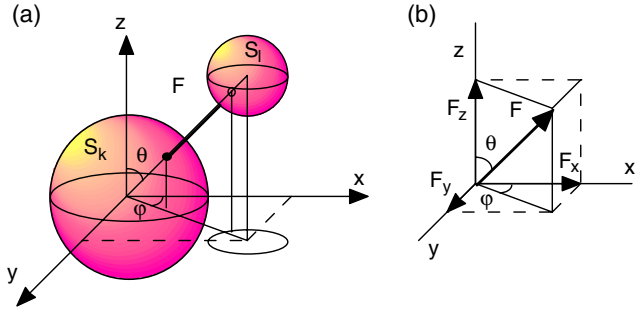

Fig. 2. Representation of a pair of interacting spheres (a) and of the interparticle force in Cartesian and spherical coordinates (b).

It does not reflect the Bingham yield stress obtained by extrapolation of the high shear range of a flow curve. In that case, the stress is not applied only to the solid so that the denominator in Eq. (18) would in principle not be needed. In the rest of this paper, which discusses yield stress values determined not by the Bingham model but by the vane technique, we proceed with Eq. (18).

(D) Subsistence Probability: Having introduced this relation to the solids volume fraction, we must now evaluate the number of configurations where bonds cannot be broken by the applied shear. In doing so, care must be exercised in the evaluation of an average value of the θ and φ.

We begin by considering bonds with fixed angles φ and determine the critical angle $\theta_{c(\varphi)}$, which satisfies Eq. (17). We can write this as

$$\tan\theta_{c(\varphi)} = \left\{ \left(\frac{G_{\max}}{\tau R_{v,50}} (\phi - \phi_0) \right)^{-1} \frac{\pi\left(b_k^2 + b_l^2\right)}{3\tilde{b}} \frac{1}{\cos\varphi} \right\} \quad (19)$$

This angle $\theta_{c(\varphi)}$ can be used to determine the subsistence probability $f_{k,l,\varphi}$ (G/τ) for a doublet with φ as the initial orientation

$$f_{k,l,\varphi} = \frac{\pi/2 - \theta_{c(\varphi)}}{\pi/2} = 1 - \frac{2\theta_{c(\varphi)}}{\pi} \quad (20)$$

The average subsistence probability (no longer dependent on the initial value of φ) is given by

$$\begin{aligned} f_{k,l} &= 1 - \frac{\int_0^{\pi/2} 2\arctan\left\{ \left(\frac{G_{\max}}{\tau R_{v,50}} (\phi - \phi_0) \right)^{-1} \frac{\pi\left(b_k^2 + b_l^2\right)}{3\tilde{b}} \frac{1}{\cos\varphi} \right\} d\varphi}{\pi \int_0^{\pi/2} d\varphi} \\ &= 1 - \frac{4}{\pi^2} \int_0^{\pi/2} \arctan\left\{ \frac{\alpha}{\cos\varphi} \right\} d\varphi \end{aligned} \quad (21)$$

where

$$\alpha = \frac{\pi}{3} \left(\frac{G_{\max}}{\tau R_{v,50}} (\phi - \phi_0) \right)^{-1} \frac{\left(b_k^2 + b_l^2\right)}{\tilde{b}}$$

If α is sufficiently large, this simplifies to

$$f_{k,l} \tilde{=} \frac{12}{\pi^3} \left(\frac{\tilde{b}}{\left(b_k^2 + b_l^2\right)} \right) \left(\frac{G_{\max}}{\tau R_{v,50}} \right) (\phi - \phi_0) \quad (22)$$

indicating that the subsistence probability is proportional to the maximum interparticle force parameter and inversely proportional to the applied shear stress. The validity of this approximation will be examined later.

(3) Volume Fraction of Solids or Maximum Packing Change

(A) General Statement: We now wish to develop an expression for Δφ, the increase in effective volume fraction of solids (or decrease in maximum packing) that arises from subsisting doublets. For this, we define $\Delta V_{k,l}$, the volume increment contributed by each subsisting doublet. For the time being, we do not need to worry about the exact expression for $\Delta V_{k,l}$; this will be discussed at the end of this section.

Let us consider a periodic system of cubic boxes with sizes sufficiently large to avoid image effects (i.e., particles interacting with themselves because of the periodic boundary condition and a very small box to particle size ratio). In each box, we identify all the contacts between particles k and l as $N_{k,l}$. The increase in volume fraction of solids from unbroken bonds is then written as

$$\Delta\phi = \frac{1}{d^3} \sum_{k=1}^{m} \sum_{l=k}^{m} N_{k,l,\phi} f_{k,l} \Delta V_{k,l} \quad (23)$$

where $N_{k,l,\phi}$ is the number of contacts between particles of size a_k and particles of size a_l at a volume fraction φ of solids phase and d^3 is the box volume.

Substitution of Eq. (22) into Eq. (23) leads to

$$\Delta\phi = \frac{6}{d^3\pi^3} \left(\frac{G_{\max}}{\tau R_{v,50}} \right) (\phi - \phi_0) \sum_{k=1}^{m} \sum_{l=k}^{m} N_{k,l,\phi} g_{k,l} \Delta V_{k,l} \quad (24)$$

where $g_{k,l}$ is dimensionless and is given by

$$g_{k,l} = 2 \frac{\tilde{b}}{\left(b_k^2 + b_l^2\right)} \quad (25)$$

(B) Coordination Number: In order to eliminate the dependence on the box size, we write this expression using t he coordination number $C_{k,l,\phi}$, which gives the number of contacts between a particle of size a_k and particles of size a_l at a volume fraction φ. It is related to the number of contacts in a box by

$$N_{k,l,\phi} = n_k C_{k,l,\phi} \begin{pmatrix} 1 & \text{if } k \neq l \\ \frac{1}{2} & \text{if } k = l \end{pmatrix} \quad (26)$$

where n_k is the number of particles of size a_k in the box of volume d^3. For spherical particles, it is given by

$$n_k = \frac{3d^3}{4\pi} \phi \frac{\phi_k}{a_k^3} \quad (27)$$

where ϕ_k is the fraction of particles of size a_k within the powder.

Substitution of Eqs. (26) and (27) into Eq. (24) leads to

$$\begin{aligned} \Delta\phi = {} & \frac{9}{2\pi^4} \left(\frac{G_{\max}}{\tau R_{v,50}} \right) \phi(\phi - \phi_0) \\ & \times \sum_{k=1}^{m} \phi_k \sum_{l=k}^{m}{}' C_{k,l,\phi} \frac{\Delta v_{k,l}}{b_k^3} g_{k,l} \end{aligned} \quad (28)$$

where the $'$ in the second summation indicates that when $k = l$, a factor of 1/2 is needed to not double count the contacts within a given size class; $\Delta v_{k,l}$ is the normalized counter part of $\Delta V_{k,l}$.

For convenience, this may also be written as

$$\begin{aligned} \Delta\phi = {} & \frac{9}{2\pi^4} \left(\frac{G_{\max}}{\tau R_{v,50}} \right) \phi(\phi - \phi_0) \\ & \times \sum_{k=1}^{m} \phi_k \sum_{l=1}^{m} \frac{C_{k,l,\phi}}{2} \frac{\Delta v_{k,l}}{b_k^3} g_{k,l} \end{aligned} \quad (29)$$

The coordination number varies with the solids volume fraction.

In fact, for a given distribution, we calculated the coordination number and found it to vary more or less linearly with the solids volume fraction. So we can write it as a function $C_{k,l}^{\max}$, the coordination at the maximum $\phi_{\max}$:

$$C_{k,l,\phi} = C_{k,l}^{\max} \frac{\phi}{\phi_{\max}} \quad (30)$$

Work by Suzuki and Oshima[25] has led to expressions for $C_{k,l}^{\max}$ given by

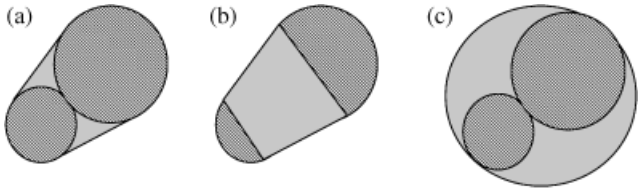

Fig. 3. Geometrical choice of effective volume fraction of solids, or maximum packing: (a) truncated cone without the particle portion, (b) truncated cone case with the particle volume, (c) enclosing sphere model without the particle volume.

$$C_{k,l}^{\max} = \beta \frac{A_s}{A_c} S_{a,l} \tag{31}$$

where

$$\frac{A_s}{A_c} = \frac{2(b_l + b_k)}{b_k + b_l - \sqrt{b_k(b_k + 2b_l)}} \tag{32}$$

and

$$S_{a,l} = \frac{\phi_l / b_l}{\sum_{i=1}^{m} \phi_i / b_i} \tag{33}$$

where $S_{a,l}$ is the fractional surface of particle of size a_l and β is a proportionality constant that Suzuki and Oshima give as 0.4.[25]

Our initial treatment used numerical calculation of particles placed at random in such a box.[26] However, we found that the above analytical expression gave rather similar results. Without giving more details on this side result, we proceed using the analytical expressions in Eqs. (31)–(33) for their enhanced convenience. This leads to

$$\Delta\phi = \frac{9\beta}{2\pi^4} \frac{\phi^2(\phi - \phi_0)}{\phi_{\max}} \left(\frac{G_{\max}}{\tau R_{v,50}}\right) F_{\sigma,\Delta} \tag{34}$$

with

$$F_{\sigma,\Delta} = \frac{1}{2} \sum_{k=1}^{m} \phi_k \sum_{l=1}^{m} S_{a,l} \frac{A_s}{A_c} \frac{\Delta v_{k,l}}{b_k^3} g_{k,l} \tag{35}$$

which accounts for the effect of particle size distribution on yield stress at constant $R_{v,50}$.

An alternative expression for Eq. (34) is obtained if we only consider the contacts of particles involved in the percolating network. Under such a condition, Eq. (27) would be written as

$$n_k = \frac{3d^3}{4\pi} (\phi - \phi_0) \frac{\phi_k}{a_k^3} \tag{36}$$

which would yield

$$\Delta\phi = \frac{9\beta}{2\pi^4} \frac{\phi(\phi - \phi_0)^2}{\phi_{\max}} \left(\frac{G_{\max}}{\tau R_{v,50}}\right) F_{\sigma,\Delta} \tag{37}$$

(C) Expression for the Lost Volume: The choice of the expression for $\Delta v_{k,l}$ is somewhat arbitrary. We have approached the problem from a geometrical point of view to include a dependence of the sizes of both particles involved in the subsisting doublets. In doing so, we tried to identify criteria that, in our opinion, would give a reasonable increment. Clearly, this represents a delicate step. The three situations we have considered are as follows:

(a) A truncated cone that is tangent to both spheres and has its base at the tangency points of these spheres. In this case, we used the entire cone volume (Fig. 3(a)). Only the volume that is not included in the particles is counted.

(b) The same situation as above but the volume of solids inside this cone is counted in the increment (Fig. 3(b)).

(c) A sphere that has a diameter equal to the sum of the diameters of both particles. Here, we do not include the particle volume included by this sphere (Fig. 3(c)).

The expressions for $v_{k,l}$ are given in Table II. The same table also contains the values of $u_{k,l}$. When $k = l$, we have the monodisperse limit for $F_{\sigma,v}$. This in turn can be used to introduce a normalized size distribution function $f_{\sigma,v}$ which is unity for monodisperse systems:

$$f_{\sigma,\Delta} = \frac{F_{\sigma,\Delta}}{u_{k,k}} \tag{38}$$

where the values of $u_{k,k}$ are given in Table II for the different geometrical models.

At this stage, it is also convenient to distinguish the case of spherical particles from the case where contact points are roughly spherical but not the particles themselves. In this latter case, $\tilde{b}$ is a constant and it is therefore more convenient to define the normalized size distribution function as

$$f_{\sigma,\Delta}^{*} = \frac{F_{\sigma,\Delta}}{u_{k,k}\tilde{b}} = \frac{F_{\sigma,\Delta}}{u_{k,k}} \frac{R_{v,50}}{a^*} \tag{39}$$

where as a reminder a* is the average radius of curvature at particle contact.

(4) Basic Yield Expression

Equation (34) is the basis for determining yield stress. The basic statement is that the suspension begins to yield once $\Delta\phi = \phi_{\max} - \phi$, where $\phi_{\max}$ is the maximum packing fraction. Thus, we can write the yield stress as

$$\tau = m_1 \frac{\phi^2(\phi - \phi_0)}{\phi_{\max}(\phi_{\max} - \phi)} \tag{40}$$

where the term m_1 is introduced for convenience and incorporates everything that is not dependent on the volume fraction of solids. With the value of 0.4 for β,[25] we get:

$$m_1 = \frac{1.8}{\pi^4} \left(\frac{G_{\max}}{R_{v,50}}\right) F_{\sigma,\Delta} \tag{41}$$

It is worth noting that the effect of particle size distribution is accounted for by the ratio $F_{\sigma,\Delta}/R_{v,50}$, and that both must be derived from the same type of distribution (e.g., surface or volume). For instance, if a median surface radius were used in place

Table II. Expressions for the Volume Increment, Limit Value of $u_{k,l}$, and Expression of the Normalized Size Distribution Function for the Three Volume Models Proposed

	Volume increment	Limit value	Normalized function
Truncated cone (without particle fraction)	$\Delta v_{k,l} = \frac{4\pi}{3} \frac{(2b_k b_l)^2}{(b_k + b_l)}$	$u_{k,k} = \frac{4\pi}{3(2-\sqrt{3})}$	$f_{\sigma,v} = F_{\sigma,v} \frac{3(2-\sqrt{3})}{4\pi}$
Truncated cone	$\Delta v_{k,l} = \frac{16\pi}{3} \frac{(b_k b_l)^2}{(b_k + b_l)^3} \left(b_k^2 + b_l^2 + b_k b_l\right)$	$u_{k,k} = \frac{4\pi}{2-\sqrt{3}}$	$f_{\sigma,v} = F_{\sigma,v} \frac{2-\sqrt{3}}{4\pi}$
Enclosing sphere	$\Delta v_{k,l} = 4\pi(b_k b_l)(b_k + b_l)$	$u_{k,k} = \frac{16\pi}{2-\sqrt{3}}$	$f_{\sigma,v} = F_{\sigma,v} \frac{2-\sqrt{3}}{16\pi}$

of the median volume radius $R_{v,50}$, then a distribution in surface rather than volume would have to be used when determining $F_{\sigma,\Delta}$. Overall, however, the ratio $F_{\sigma,\Delta}/R_{v,50}$ should be independent of this choice. The advantage of this approach with respect to the Kapur model is that we do not have to determine which average radius is most appropriate. The inconvenience is that it requires an accurate determination of the particle size distribution.

Other than this, we note that when percolation is taken into account in the coordination number determination, we obtain

$$\tau = m_1 \frac{\phi(\phi - \phi_0)^2}{\phi_{max}(\phi_{max} - \phi)} \tag{42}$$

Both Eqs. (40) and (42) indicate that the yield stress should vary inversely with the median particle size. The effect of the size distribution is buried in $F_{\sigma,\Delta}$ and although its absolute value depends on the choice of $\Delta v_{k,l}$, its variation with σ is relatively independent of the different volume increment geometric models.

IV. Results

(1) Volume Fraction Dependence

The model developed above is now tested using the previously discussed data of Zhou *et al.*[19] on alumina suspensions. We only examine data at the IEP, because this includes all the microstructural information we need. These data are concerned with four powders at several volume fractions of the solid phase.

They are plotted as a function of volume fraction of solids, and fitted using both Eqs. (40) and (42). In all cases, both equations provided very good fits with percolation thresholds close to zero (between 0.024 and 0.040) and similar maximum packing fractions (between 0.57 and 0.59). We then proceeded to fit the four data sets using Eq. (42), using the same maximum packing and percolation threshold, which yielded 0.57 and 0.026, respectively. Again, the fitting was excellent, as can be seen in Fig. 4 both on the linear scale (a) and the log–log scale (b).

Further evaluation of the quality of the fit was performed through the following normalization procedure. Each yield stress value was divided by the volume fraction function from Eq. (42) $\left(\phi(\phi - \phi_0)^2/\phi_{max}(\phi_{max} - \phi)\right)$. This gives a data set for each powder that is independent of volume fraction and its scatter is indicative of the quality of the fit. In order to compare the errors among the powders on a similar scale, each series was normalized to its average. As a result, data scatter around unity indicates how well or badly the data are represented by the YODEL. As can be seen in Fig. 5, this scatter is independent of volume fraction and is only on the order of $\pm$15–20%.

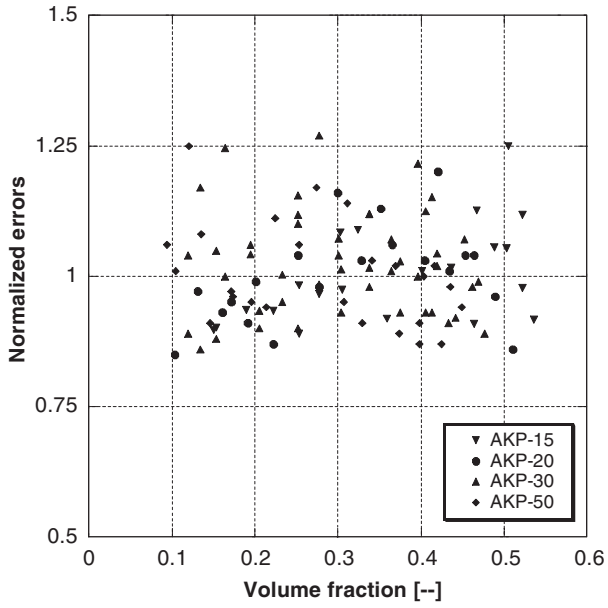

Fig. 5. Normalized yield stress values showing no dependence on volume fraction of solids and limited scatter around the average.

(2) Particle Size Dependence

As described above, the fitted curves in Fig. 4 all use the same maximum packing fraction and percolation threshold. In addition, each of them has a distinct prefactor m_1, as defined in Eq. (41). Combining Eqs. (5), (41), and (38), and, for spherical particles, we obtain

$$m_1 = \frac{0.15 u_{k,k} A_0}{\pi^4 H^2} \frac{f_{\sigma,\Delta}}{R_{v,50}} \tag{43}$$

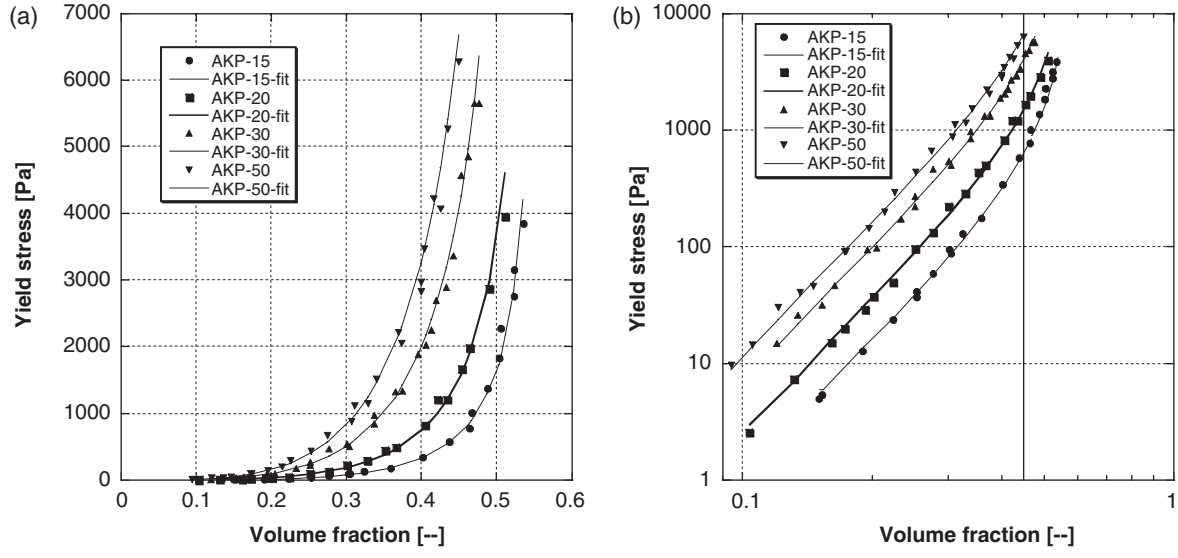

Fig. 4. Yield stress data of suspensions with four alumina powders at the IEP. The data from Zhou *et al.*[19] are marked with symbols. The lines indicate the fit obtained with Eq. (42), using the same maximum packing (0.57) and percolation threshold (0.026). In the figure to the left, a double log scale is used, which suggests a power-law fit to be adequate up to volume fractions of about 0.43 marked by the vertical line in accordance with a former treatment of this data.[19]

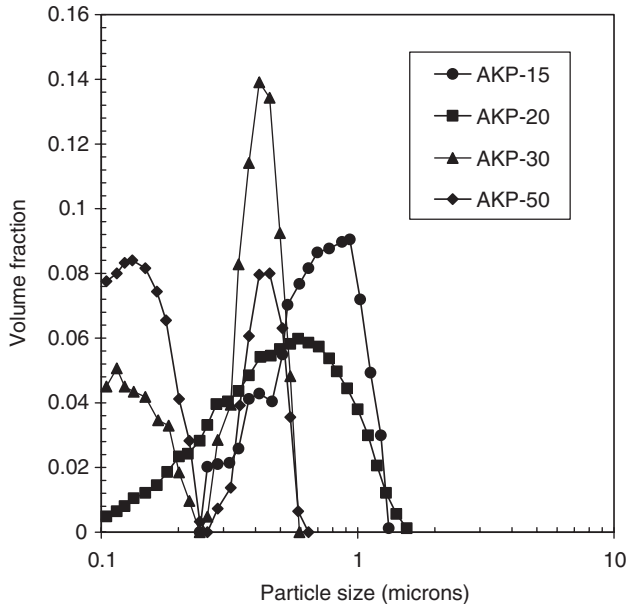

Fig. 6. Particle size distributions measured by the coulter counter method.[27]

or using Eq. (39), for nonspherical particles with spherical contact points we obtain

$$m_1 = \frac{0.15 u_{k,k} A_0 a^*}{\pi^4 H^2} \frac{f^*_{\sigma,\Delta}}{R^2_{v,50}} \tag{44}$$

The analysis of Zhou *et al.* suggests that the value of H is the same for all four powders. Thus we expect m_1 to be proportional to either $f_{\sigma,\Delta}/R_{v,50}$ or $f^*_{\sigma,\Delta}/R^2_{v,50}$. We emphasize once again that these terms are independent of any definition of an average particle size (number, surface or volume). We chose to normalize values by $R_{v,50}$, but could have done the same for another average provided $f_{\sigma,\Delta}$ and $f^*_{\sigma,\Delta}$ are calculated with the corresponding normalized particle sizes.

The particle size distribution of the powders considered is given in the thesis of Zhou.[27] Using these (Fig. 6), we have calculated $R_{v,50}$, $f_{\sigma,\Delta}$, $f^*_{\sigma,\Delta}$, and R_S, the surface average radius.

The values reported in Table III indicate that for all powders, $f_{\sigma,v}$ is close to unity. For $f^*_{\sigma,\Delta}$, values differ much more from powder to powder. Another observation is that differences because of the geometrical model for $\Delta v_{k,l}$ were small. With the values of $f_{\sigma,v}$ and $f^*_{\sigma,\Delta}$ in Table III, we can plot m_1 versus $f_{\sigma,\Delta}/R_{v,50}$ and $f^*_{\sigma,\Delta}/R^2_{v,50}$ (Figs. 7(a) and (b)).

Let us begin examining the correlation of Fig. 7(a). There is a linear relation between m_1 and $f_{\sigma,\Delta}/R_{v,50}$; however, it does not go through the origin. The reason for this is not clear. Nevertheless, we proceed to examine whether we obtain a correct estimate of the minimum separation distance H based on the slope of the linear regression (dashed line in Fig. 7(a)) and Eq. (43). With a Hamaker constant of 5.3×10^{-20} J, the same as used by Zhou *et al.*,[21] we obtain values of H of 2.1 and 4.3 nm for the truncated cone and sphere respectively. If we use a linear fit forced through the origin (continuous line in Fig. 7(a)), we obtain 2.4 and 5.4 nm, respectively. Overall, all these values are in rather good agreement with those reported in Table I, considering that the relation between m_1 and $f_{\sigma,\Delta}/R_{v,50}$ is not correctly predicted by the YODEL.

Table III. Size Distribution Information on the Alumina Powders,[19] Giving Surface Average Radius R_s, Mean Volume Radius $R_{v,50}$ and the Particle Size Distribution Function $f_{\sigma,\Delta}$ and $f^*_{\sigma,\Delta}$ for the Truncated Cone and Enclosing Sphere Volume Increments (Figs. 3(b) and (c))

		AKP-15	AKP-20	AKP-30	AKP-50
R_s		0.290	0.201	0.124	0.093
$R_{v,50}$		0.325	0.245	0.175	0.084
fpsd	Cone	0.96	0.98	1.14	0.78
	Sphere	1.01	1.08	1.25	0.83
f*psd	Cone	1.21	1.70	2.23	0.90
	Sphere	1.28	1.88	2.43	0.94

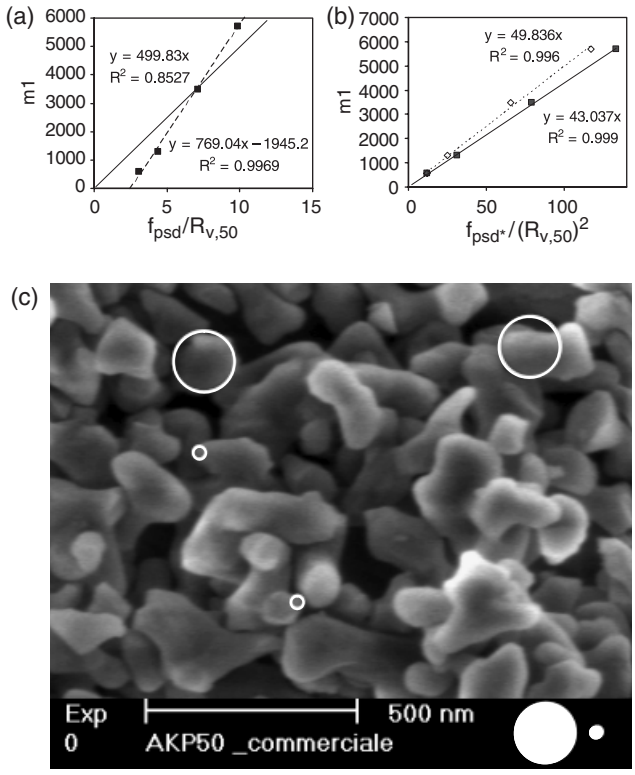

Fig. 7. Correlation of fitting parameter m_1 with particle size: (a) spherical particles, (b) filled symbols, particles with fixed radius of curvature at contact points. Open symbols correlate m_1 with $1/R^2_S$. Values are for the enclosing sphere case (Fig. 3(c)). Very similar degrees of correlation are obtained with the cone models (Figs. 3(a) and (b)). (c). High-resolution scanning electron micrograph of AKP-50 showing the extremes of radii of curvature at particle contacts (140 and 34 nm) with the white circles, as discussed in the last paragraph of Section *IV(2)*.

If we now examine Fig. 7(b), we can see that there is a linear relation between m_1 and $f^*_{\sigma,\Delta}/R^2_{v,50}$ passing through the origin. This is in complete agreement with Eq. (44), and supports the idea that the magnitude of the interparticle forces is best represented by a characteristic radius of curvature a^* at contact points and that this characteristic curvature is the same for the four powders considered. It is also in general agreement with the scaling of yield stress with $1/R^2_S$ found by Zhou *et al.* In fact, in Fig. 7(b), the open symbols, which also show a linear trend, correspond to values of m_1 plotted versus $1/R^2_S$.

In this case, we are faced with the problem that we cannot estimate H without defining a^*. A way around this is to use the average value of H obtained by Zhou *et al.* (2.4 nm) from the dependence of yield stress on the zeta potential. With the same Hamaker constant as before, we find that the a^* would be 73 nm for the cone and 17 nm for the sphere volume increment models, and is coherent with high-resolution scanning electron micrographs (Fig. 7(c)). In Fig. 7(c), circles of diameter 34 and 140 nm corresponding to contact points with spherical radii of curvature of 17 and 70 nm for a* are marked. This corresponds, respectively, to 80% and 20% of the value of R_S for AKP-50, which is the finest powder. The correlation coefficient for the spherical

case is slightly better than that for the cones (0.999 with respect to 0.998), and both are slightly better than the scaling with respect to $1/R_S^2$ (0.996). We also note that diameters using the truncated cone model without particle volume (Fig. 3(a)) are in the range of 250 nm, which is too large and therefore this geometry is not discussed further in this paper.

V. Discussion

(1) Volume Fraction Dependence

The dependence on solids volume fraction of the yield stress of fitted these alumina suspensions is very well predicted by our model, as illustrated in Fig. 4. We emphasize that all curves could be fitted using the same value of percolation threshold and maximum packing. This appears reasonable as all these powders have narrow size distributions and similar shapes. In contrast to former treatment of these data,[19] our function covers the entire range of volume fractions.

We must, however, state that in the low range of volume fractions of solids ($\phi < 0.25$), models considering for instance the fractal nature of agglomerates or the role loops[28,29] on modulus may be more relevant than the YODEL. Thus, we will not attempt to justify the value of the estimated percolation threshold.

(A) Maximum Packing: For most situations of practical interest in the processing of ceramics and cementitious materials, it is the high end of volume fractions of solids ($\phi > 0.25$) that is of interest. In this range the influence of percolation threshold, fractal dimension, or specific microstructural features is small and we can write

$$\tau \cong m_1 \frac{\phi^3}{\phi_{max}(\phi_{max} - \phi)} \tag{45}$$

For the percolation threshold estimated, the error induced using the above equation is less than 20% when the volume fraction of solids in suspension is larger than 0.25. Thus, for many cases of practical interest, the only fitting parameters are m_1, which is linked to interparticle forces, and the maximum packing.

In order to further test the pertinence of our model, we have attempted an independent estimation of the maximum packing fraction of one of the powders. For this, we have considered that the vane test used to determine the yield stress values discussed in this paper induces very low shear rates. Thus, we have carried out filter-pressing experiments and then extrapolated the data back to zero pressure in order to estimate a maximum packing most relevant to the testing conditions. This was done with the AKP-50. A suspension was prepared at a solids volume fraction of 0.39, pH ~ 7.3, and sonicated for 15 min. It was then introduced into a filter press on an Instron loading machine. Loads were applied as follows: 1.6 MPa (4 h), 3.2 MPa (4 h), 4.8 MPa (2 h), 6.4 MPa (2 h), 12.9 MPa (1 h), 25.8 MPa (1 h), and 32.2 MPa (1 h). After this, the load was progressively released to determine the elastic deformation of the compressed particle network. Apart from the lowest load, all other combinations of load and duration were sufficient to reach equilibrium piston displacement from which the packing at the given load could be determined. The data are plotted in Fig. 8, and are well represented by a hyperbolic function starting at a non zero packing fraction. The two data series correspond to the compressed (loading) and relaxed (unloading) particle networks. Both give a similar estimate of the packing fraction at zero load.

The value of the maximum packing obtained from Fig. 8 is about 0.585, while our average fit gave 0.57 and the direct fit of the AKP-50 powder alone gave 0.59. Thus, the maximum packing in the YODEL should not be viewed as a fitting factor, but rather as a physical variable that can be determined by an independent experiment.

For this reason, we also evaluate the YODEL in its simplest form, neglecting percolation threshold and taking the maximum packing obtained by filter pressing. We calculate the normalized errors as for Fig. 5. As a reminder, the scatter of these errors around unity is indicative of how well or badly the volume fraction dependence of yield stress is captured by the model. The results in Fig. 9(a) indicate a drift of these errors with volume fraction in contrast with Fig. 5. However, we also note that for AKP-50 (filled symbols), which is the powder whose maximum packing was measured, the drift above volume fractions of 0.25 is negligible. This corresponds to the zone where the percolation threshold effect is lost. For this reason, we constructed another plot only fitting data with volume fractions of solid in excess of 0.25. The normalized errors in Fig. 9(b) now do not indicate any significant drift and are in the range of ± 15–20%. Note that in these plots, each powder is fitted with a single parameter m_1, which depends on interparticle forces and particle sizes.

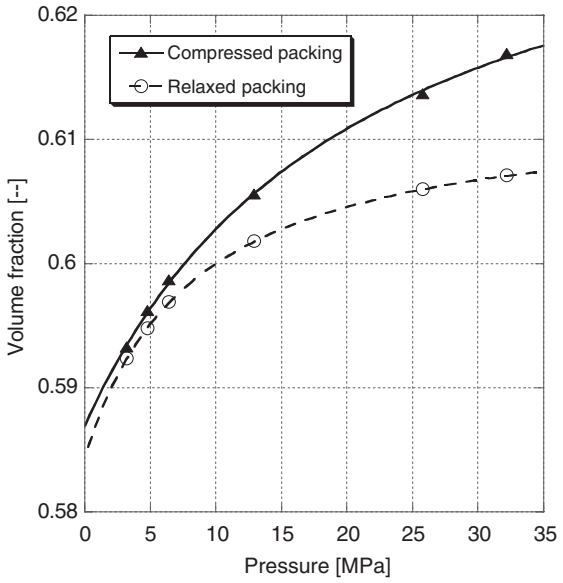

Fig. 8. Packing fraction obtained by filter pressing of AKP-50 as a function of the pressure applied to the particle network.

(2) Particle Size Dependence

In the presentation of the YODEL, we have considered two situations for interparticle forces. The first situation assimilates particles to spheres and uses the classical result showing a scaling of interparticle forces with the first power of the particle size. With this choice for interparticle forces, we predict that the yield stress should scale with the inverse first power of particle size. In this respect, we obtain a result similar to Kapur *et al.*[2]

In contrast, we have also considered the case where although curvature at particle contacts may be spherical, it is not proportional to particle size. This would be the case for a given surface roughness or a characteristic morphology of a set of powders (e.g., the case in question for the AKP aluminas).

In the first case, we expect the prefactor m_1, obtained from the fit of yield stress versus volume fraction, to be proportional to $f_{\sigma,\Delta}/R_{v,50}$. In the second case, we expect m_1 to be proportional to $f^*_{\sigma,\Delta}/R^2_{v,50}$. Using the measured particle size distributions, we found that the second case gives the best agreement and that this scaling ends up being quite similar to the one proposed by Zhou *et al.*[20] ($1/R_s^2$). As the value of the characteristic radius of curvature at particle contact, a^*, is not known, this prevents us from calculating the minimum separation distance, H, from the slope in Fig. 7(b). We have calculated the value that a^* would have to have in order to obtain a value of H consistent with those reported in Table I. These values, when compared with HRSEM images (Fig. 7(c)), indicate that we are dealing with a characteristic morphological feature of these powders rather than a surface roughness. A very schematic representation of this is given in Fig. 10. It is meant to illustrate that the number of contacts continues to scale with particle size (left and right col-

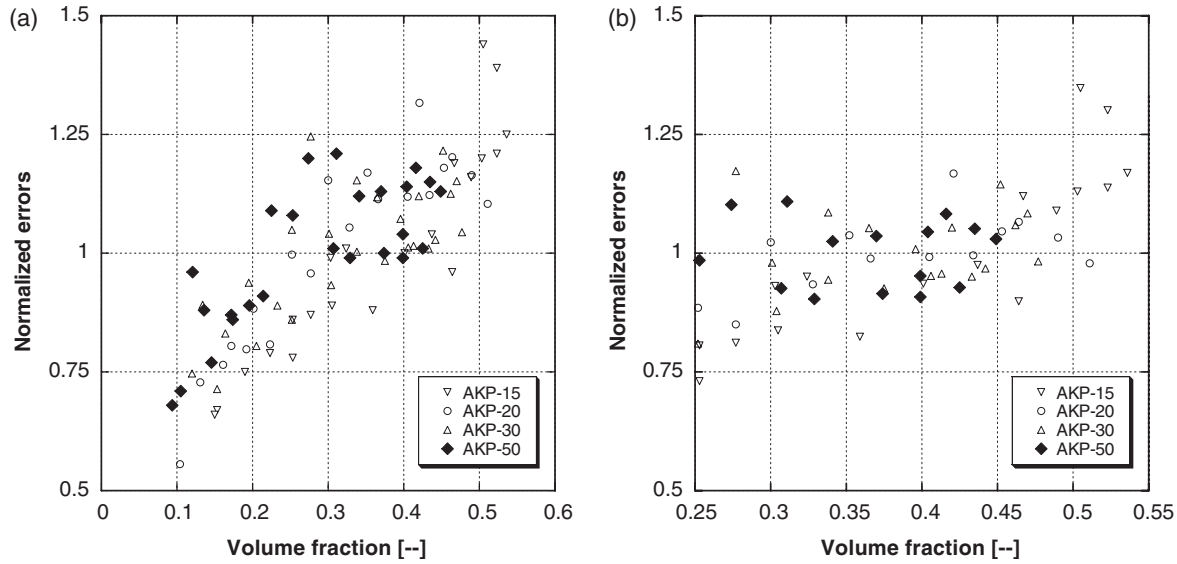

Fig. 9. Normalized yield stress for the prediction of the yield stress dependence on the volume fraction of solids: (a) neglecting percolation threshold and using the maximum packing estimated from filter pressing, (b) for volume fractions of solids >0.25.

umn), while in one case (upper line) the interparticle forces would be proportional to particle size and in the other (bottom line) they would be largely independent of particle size.

The fact that these values of a^* are close to the particle sizes of the powders considered probably explains why the estimate of H based on the linear regressions of m_1 versus $f_{\sigma,\Delta}/R_{v,50}$ provided a reasonable estimate of H. Therefore, overall, we believe that for this set of powders, the interparticle forces are probably better approximated using a fixed radius of curvature than the particle size. Nevertheless, we cannot completely discard the possibility that the YODEL does not capture an effect that leads to a non-zero intercept of the linear relation between m_1 and $f_{\sigma,\Delta}/R_{v,50}$ also observed.

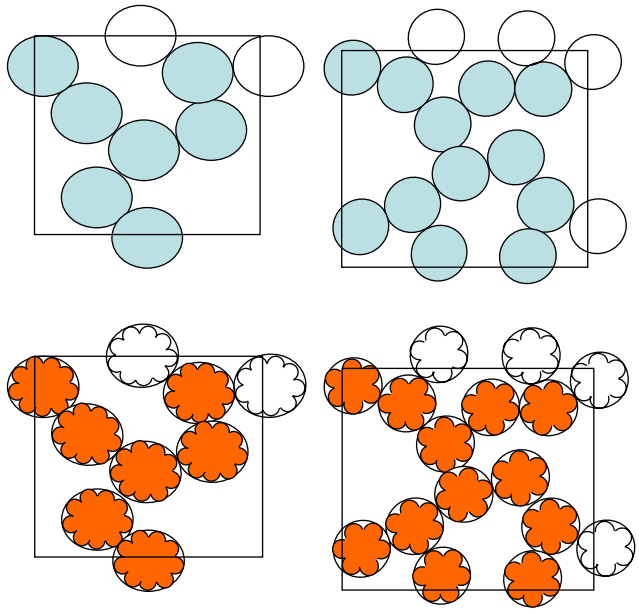

Fig. 10. Schematic illustration of a possible reason for the variable dependence of yield stress on particle size. The upper case would correspond to interparticle forces scaling with the particle radius. The bottom case would correspond to particles with a characteristic radius of curvature at particle contacts that is independent of particle size. In both cases, the number of contacts scale with the inverse square particle size, but the forces scale in one instance with particle size and the other independent of it.

(3) Validity of Approximations

The above results use the approximation in Eq. (22) to obtain the subsistence probability. In fact, this is not necessary but convenient as numerical integration of Eq. (21) is possible. However, it would no longer provide a simple explicit and convenient expression of yield stress as a function of the interparticle force parameter and solids volume fraction. As mentioned previously, the approximation is valid for large values of α.

In the case that appears most relevant to the powders considered in this paper, virtually all data can be analyzed in this simplified way if the enclosing sphere geometrical model for the volume increment is used. For the cone model, the approximation would only hold for volume fractions of solids above about 0.25 if we accept a 25% error. If we were to consider the situation where $f_{\sigma,\Delta}$ were to be used rather than $f^*_{\sigma,\Delta}$, the lowest acceptable volume fraction of solids would be even higher (about 0.35).

We emphasize that these limits are powder specific and that, overall, the simplified expressions we have presented become increasingly accurate as volume fraction increases. This is of particular interest for many applications for the processing of ceramics or cementitious systems. Moreover, in the case of the powders considered here, the simplified expressions appear to be generally acceptable.

(4) Advantages and Limitations of the YODEL

The YODEL as presented here seems to capture very well the dependence of yield stress on volume fractions over a very broad range of volume fractions. The functionality of this dependence involves a geometrical maximum packing, a percolation threshold, and a prefactor that depends on interparticle forces and particle sizes. In most cases of interest to the processing of ceramics and cementitious materials, the volume fractions are high enough for the role of percolation threshold to be overlooked. Furthermore, we were able to show that the maximum packing can be estimated by an independent measurement and is therefore not to be treated as a fitting parameter. Thus, one of the YODEL strengths appears to be the volume fraction dependence that it proposes.

The remaining fitting parameter that we noted, m_1, depends on particle size, size distribution, shape, and interparticle forces. For a given powder, it could be used to scale relations of interparticle forces. In the present case, where different powders were used, all these factors could be expected to vary from powder to powder. Our results suggest that the issue of shape could be a key factor for interparticle force formulation. More specifically,

the scaling of m_1 with particle size (and size distribution) suggests that the interparticle forces do not depend on particle size for this set of powders. We have attempted to rationalize this by indicating that these particles, which are clearly not spherical, might have contact points with similar ranges of radius of curvature. Indirectly, the fact that the effect of particle size distribution is better captured using this hypothesis tends to support this idea.

Unfortunately, this assumption limits the generality of the model. It is, however, not completely inconsistent with the fact that the different scaling relations of yield stress with particle size can be found in the literature with powers from 1 to 3. From our results in this paper, we can suggest that powders with similar surface features may, in certain cases, be modeled with a fixed average radius of curvature at particle contacts. This may, for instance, be the case for cements, which would mean that the use of the YODEL could remain rather general for such systems.

We should also point out that for this set of powders, the minimum separation distance was shown to be the same. This cannot be expected to be a universal result. In some cases, particles may have a small surface roughness, whose effect may end up somewhat increasing the average minimum separation distance. Furthermore, if this were the case, and if this surface roughness were proportional to the particle size, the dependence of yield stress on particle size would change once again. Provided a global spherical curvature could be used on such particles, we would then obtain yield stresses that would in principle scale with the inverse third power of particle size. Such issues must not be overlooked if one wishes to compare the role of particle size on powders of different types and origins. The approach used by Zhou *et al.* to plot normalized yield stress appears to be a very elegant way of determining whether the minimum separation distance is dependent or not on particle size. For these alumina powders, there was no size dependence and that allowed us to carry out the more extensive analysis outlined in this paper.

It is also worth emphasizing that if one is interested in studying changes in interparticle forces and volume fraction effects, then the use of a single powder, together with the YODEL, should allow the extraction of proper scaling relations, although not the absolute values of minimum separation distances.

In the specific case of these AKP powders, we have attempted to estimate the value of the characteristic radius of curvature at particle contacts, a^*. Depending on the model used, this turns out to be between 20 and 80 nm for the enclosing sphere and truncated cone volume increment models, respectively. These should not be taken as exact values but rather as ranges, because of other issues linked to the nonsphericity of these particles (the number of contacts and the value of the incremental volume). Despite these limitations, we used these values of a^* to confirm that an approximation used in the derivation of the YODEL was acceptable for most if not all the data considered. More generally, the acceptability of this approximation, which allows us to obtain an explicit expression for yield stress, increases with volume fraction. Once again, this makes the YODEL well adapted for use in describing flowing systems with high solids loadings, as found for many ceramic and cement suspensions.

Finally, we also point out that the YODEL has shown good predictability for suspensions of powder mixes (to be reported in a separate communication). The crucial aspect there is that the maximum packing fraction of mixes must be estimated based on the packing of the pure components and their relative sizes. This can be done, without introducing any additional fitting parameters, with the model of de Larrard,[30] but is beyond the scope of this paper.

VI. Conclusions

A model to describe the yield stress (YODEL) for concentrated suspensions that form an attractive network of interparticle bonds has been developed. The model attempts to take into account the microstructural contribution that arises from the size distribution of the particles. It links physical parameters (particle size, size distribution, maximum packing fraction, minimum separation distance at contact) to the shear stress needed to break down the attractive network sufficiently for it to yield.

The model predicts accurately the dependence of yield stress on volume fraction. The fitting parameters involved include the maximum packing, a percolation threshold, and a term linked to interparticle forces and particle size distribution. For most cases of practical interest, volume fractions are sufficiently high not to have to be concerned about the role of percolation threshold. In addition, a separate estimate of the maximum packing of solids was in good agreement with the value estimated from fitting the model to the experimental data of yield stress.

Analysis of the remaining fitting parameter revealed that the YODEL predicts the correct scaling of yield stress with particle size if one introduces the existence of a characteristic radius of curvature at particle contacts that is the same in the four powders examined. This introduces an additional term that, at this stage, cannot be determined by independent experiments and must be treated as a fitting factor. This compromises the generality of the model among very different non-spherical powders. However, for a set of powders of similar morphology, or for a given powder for which interparticle forces are modified, the YODEL remains valid.

We recognize that because of the very nature of this approach, perfect quantification cannot be expected. However, the amount of fitting is limited to a minimum and provides correct functionality of interparticle force, particle size, particle size distribution, volume fraction of solids, and maximum packing. Despite the remaining uncertainty on numerical prefactors, the coherence of this result appears as an encouraging step forward in this complex area of concentrated suspension rheology.

Appendix A: Log-Normal Size Distributions

Many powders, including cement, exhibit quasi–log-normal size distributions. For such cases, it may be convenient to obtain quick estimates for the value of $F_{\sigma,\Delta}$ as a function of the standard distribution of the distribution.

Let us consider log-normal distributions where we denote Δ for the solids volume fraction increment between two successive classes of particles; we have

$$\phi_k = \frac{1}{\sigma\sqrt{2\pi}} \exp\left(-\frac{1}{2}\left(\frac{\ln(b_k)}{\sigma}\right)^2\right)\Delta \tag{A-1}$$

where $\Delta = \ln(b_{k+1}/b_k)$

With this expression, $s_{a,l}$ becomes

$$\begin{aligned} S_{a,l} &= \frac{\Delta}{\sigma\sqrt{2\pi}}\frac{1}{b_l}\exp\left(-\frac{1}{2}\left(\sigma^2 + \left(\frac{\ln(b_l)}{\sigma}\right)^2\right)\right) \\ &= \frac{\Delta}{\sigma\sqrt{2\pi}}\exp\left(-\frac{1}{2}\left(\sigma + \frac{\ln(b_l)}{\sigma}\right)^2\right) \end{aligned} \tag{A-2}$$

Thus,

$$\sum_{i=1}^{\infty}\frac{\phi_i}{a_i} \cong \frac{1}{\sigma\sqrt{2\pi}}\int_{-\infty}^{\infty}\frac{\exp\left(-\frac{1}{2}\left(\frac{x-X}{\sigma}\right)^2\right)}{\exp(x)}dx = \frac{\exp\left(\frac{\sigma^2}{2}\right)}{R_v} \tag{A-3}$$

where $x = \ln(a_i)$ and $X = \ln(R_v)$

Substitution into Eq. (35) yields

$$F_{\sigma,\Delta} = \frac{\Delta^2}{\sigma^2 2\pi}$$

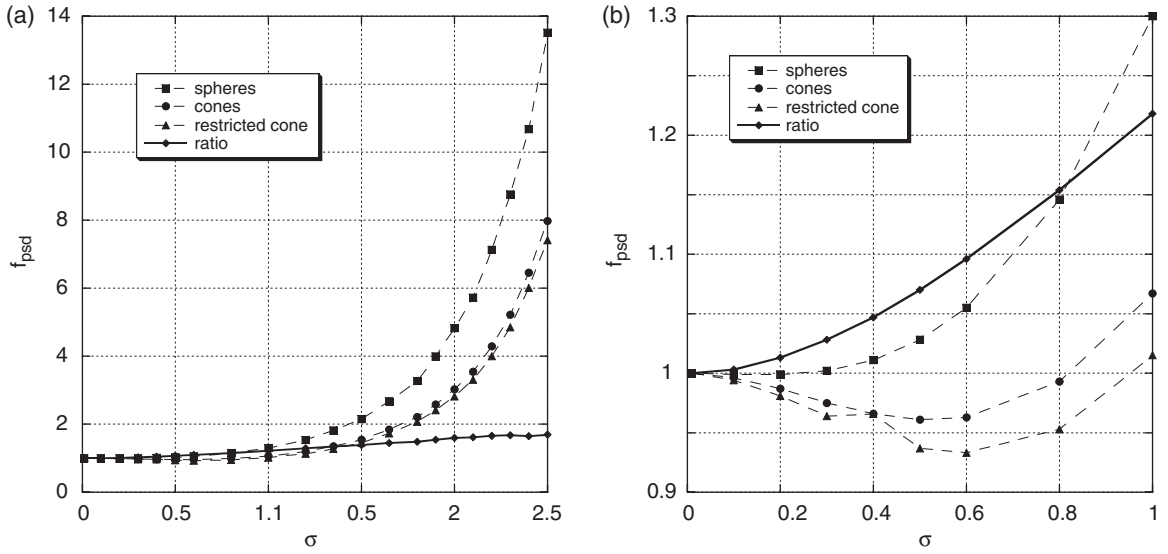

Fig. A1. Evolution of the normalized function, $f_{\sigma,v,}$ that describes the effect of particle size distribution on yield stress. The curve labeled ratio corresponds to the ratio between the values of $f_{\sigma,v}$, obtained with the sphere model (Fig. 3(c)) and those obtained with the truncated cone model (Fig. 3(b)).

$$\times\sum_{k=1}^{m}\exp\left(-\frac{1}{2}\left(\frac{\ln(b_k)}{\sigma}\right)^2\right)\sum_{l=1}^{m}\exp\left(-\frac{1}{2}\left(\sigma+\frac{\ln(b_l)}{\sigma}\right)^2\right)(u_{k,l}) \tag{A-4}$$

where

$$u_{k,l}=\frac{1}{2}\frac{A_s}{A_c}\frac{\Delta v_{k,l}}{b_k^3}g_{k,l}$$

$$=\frac{2}{b_k+b_l-\sqrt{b_k(b_k+2b_l)}}\frac{\tilde{b}(b_k+b_l)}{b_k^3\left(b_k^2+b_l^2\right)}\Delta v_{k,l} \tag{A-5}$$

and $\Delta v_{k,l}$ is the dimensionless volume increment.

Using these equations, we have calculated the values of $f_{\sigma,\Delta}$ and $f^*_{\sigma,\Delta}$ for various standard deviations. Figure A1(a) shows that for particle size distributions values of $f_{\sigma,\Delta}$ increase strongly with standard deviation larger than unity. Below unity, variations depend strongly on the model chosen, but the differences in the magnitude are small (Fig. A1(b)). For standard deviations of one, the relative increase of $f_{\sigma,\Delta}$with standard deviation is rather independent of the geometrical model selected for $\Delta v_{k,l}$. To illustrate this, the ratio between values of $f_{\sigma,\Delta}$ for the sphere (Fig. 3(b)) and the truncate cone (Fig. 3(c)) is also plotted in Fig. A1(a and b). In the extreme case plotted in Fig. A1(a), values of $f_{\sigma,\Delta}$ terms reach values of 14 and 8, respectively, and their ratio becomes 1.5. Thus, the dependence of yield stress on the standard deviation of a log-normal size distribution has only a second-order dependence on the nature of the geometrical model chosen.

For $f^*_{\sigma,\Delta}$ values are, Fig. A2, a function of standard deviation. It can be seen that this function grows faster as a function of standard deviation than $f_{\sigma,\Delta}$. In addition, as for $f_{\sigma,\Delta}$,the ratio of the values of $f^*_{\sigma,\Delta}$ for the sphere and cone shows a much smaller dependence of standard deviation.

It turns out that for these powders the cumulative distributions can be rather well fitted with log-normal distributions, and estimations of both $f_{\sigma,\Delta}/R_{v,50}$ and $f^*_{\sigma,\Delta}/R^2_{v,50}$ are in general agreement with those obtained using directly the measured particle size distribution. We have reported only values using the experimental distribution for higher accuracy and conciseness.

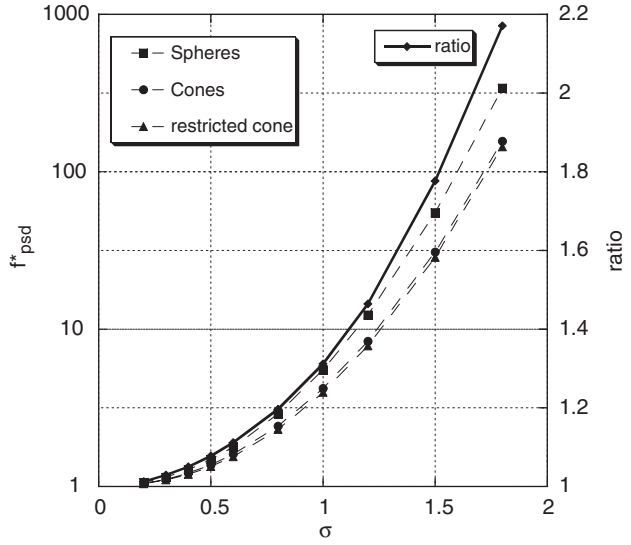

Fig. A2. Particle size distribution $f^*_{\sigma,\Delta}$ obtained for the radius of curvature at interparticle contacts is independent of particle size, as illustrated schematically in Fig. 10.

Appendix B. Comparison with a Preliminary Version of the YODEL

In a preliminary paper that does not describe the model in detail, one of us reported the following expression instead of those in Eqs. (40) and (42):[31]

$$\tau=m_1\frac{(\phi-\phi_0)^2}{\phi_{max}(\phi_{max}-\phi)} \tag{B-1}$$

This difference arises from a different accounting for percolation in the coordination number and from including the fact that below the yield point, the stress is transmitted through the solid (percolating) network, which is now expressed in Eq. (18).

Also, the fitting procedure we used fixed the maximum packing to 64%, which is not an adequate value for these powders given the test conditions. The percolation threshold values were not evaluated to be zero. In the end, this led to the same number of fitting parameters. They were m_1 and the percolation threshold.

The results also showed that m_1/f_{psd} varied linearly with $1/D_{v,50}$. However, the analysis involved a couple of inaccuracies

involving f_{psd} and should be overlooked with respect to the analysis proposed in this paper.

Acknowledgments

The authors would like to thank Prof. G.W Scherer (Princeton University, U.S.A.), Dr. Nicolas Roussel (LCPC, France) and Dr. Nicos Martys (NIST, U.S.A.) for their useful comments on this work. Special thanks are also due to M. Carlos Morais (EPFL) for the help with the filter pressing experiments and Dr. L Cristina Soare for the SEM work.

References

[1]R. Buscall, I. J. McGowan, P. D. A. Mills, R. F. Stewart, D. Sutton, L. R. White, and G. E. Yates, "The Rheology of Strongly Flocculated Suspensions," *J. Non-Newtonian Fluid Mech.*, **24**, 183–202 (1987).

[2]P. C. Kapur, P. J. Scales, D. V. Boger, and T. W. Healy, "Yield Stress of Suspensions Loaded with Size Distributed Particles," *A.I.Ch.E. J.*, **43**, 1171–9 (1997).

[3]P. J. Scales, S. B. Johnson, T. W. Healy, and P. C. Kapur, "Shear Yield Stress of Partially Flocculated Colloidal Suspensions," *A.I.Ch.E. J.*, **44** [3] 538–44 (1998).

[4]Z. Zhou, M. J. Solomon, P. Scales, and D. V. Boger, "The Yield Stress of Concentrated Flocculated Suspensions of Size Distributed Particles," *J. Rheol.*, **43** [3] 651–71 (1999).

[5]G. M. Channel and C. F. Zukoski, "Shear and Compressive Rheology of Aggregated Alumina Suspensions," *A.I.Ch.E. J.*, **43** [7] 1700–8 (1997).

[6]A. A. Potanin and W. B. Russel, "Fractal Model of Consolidation of Weakly Aggregated Colloidal Suspensions," *Phys. Rev. E*, **53** [4] 3702–9 (1996).

[7]L. Bergström, C. H. Schilling, and I. A. Aksay, "Consolidation Behavior of Flocculated Alumina Suspension," *J. Am. Ceram. Soc.*, **75** [12] 3305–14 (1992).

[8]G. V. Franks, Z. Zhou, N. J. Duin, and D. V. Boger, "Effect of Interparticle Forces on Shear Thickening of Oxide Suspensions," *J. Rheol.*, **44** [4] 759–79 (2000).

[9]M. Strauss, T. Ring, A. Bleier, and H. K. Bowen, "Coagulation in Processing of Ceramic Suspensions: Powder Size Distribution Effects," *J. Appl. Phys.*, **58** [10] 3871–9 (1985).

[10]R. J. Flatt, M. Martys, and L. Bergström, "The Rheology of Cementitious Materials," *Mat. Res. Bull.*, **29** [5] 314–8 (2004).

[11]C. Vernet, "Ultra-Durable Concretes: Structure at the Micro- and Nano-scale," *Mat. Res. Bull.*, **29** [5] 324–7 (2004).

[12]R. J. Flatt, "Dispersants in Concrete"; pp. 247–94 in *Polymers in Particulate Systems: Properties and Applications. Surfactant Science Series*, Chapter 9, Edited by V. A. Hackley, P. Somasundran, and J. A. Lewis. Marcel Dekker Inc, New York, 2001.

[13]W. M. Sigmund, N. S. Bell, and L. Bergström, "Novel Powder Processing Methods for Advanced Ceramics," *J. Am. Ceram. Soc.*, **83** [7] 1557–74 (2000).

[14]R. J. Flatt, "Dispersion Forces in Cement Suspensions," *Cem. Concr. Res.*, **34**, 399–408 (2004).

[15]L. Bergström, "Hamaker Constants of Inorganic Materials," *Adv. Colloid. Interface Sci.*, **70**, 125–69 (1997).

[16]W. B. Russell, D. A. Saville, and W. R. Schowalter, *Colloidal Dispersions*. Cambridge University Press, Cambridge, 1989.

[17]R. J. Flatt and P. Bowen, "Electrostatic Repulsion between Particles in Cement Suspensions: Domain of Validity of Linearized Poisson-Boltzmann Equation for Nonideal Electrolytes," *Cem. Concr. Res.*, **33**, 781–91 (2003).

[18]P. G. de Gennes, "Polymers at an Interface: A Simplified View," *Adv. Colloid Interfaces Sci.*, **27**, 189–209 (1987).

[19]Z. Zhou, M. J. Solomon, P. J. Scales, and D. V. Boger, "The Yield Stress of Concentrated Flocculated Suspensions of Size Distributed Particles," *J. Rheol.*, **43** [3] 651–71 (1999).

[20]Z. Zhou, P. J. Scales, and D. V. Boger, "Chemical and Physical Control of the Rheology of Concentrated Metal Oxide Suspensions," *Chem. Eng. Sci.*, **56**, 2901–20 (2001).

[21]Z. Zhou, D. V. Boger, P. J. Scales, and T. W. Healey, "Shear and Compressional Rheology Principles in Ceramic Processing"; pp. 157–95 in *Polymers in Particulate Systems: Properties and Applications*, Edited by V. A. Hackley, P. Somasundaran, and J. A. Lewis. Marcel Dekker, New York, 2001.

[22]N. Q. Dzuy and D. V. Boger, "Yield Stress Measurement for Concentrated Suspensions," *J. Rheol.*, **27** [4] 321–49 (1983).

[23]N. Q. Dzuy and D. V. Boger, "Direct Yield Stress Measurement with the Vane Method," *J. Rheol.*, **29** [3] 335–47 (1985).

[24]H. Rumpf, "The Strength of Granules and Agglomerates"; pp. 379–418 in *Agglomeration*, Edited by W. A. Knepper. Interscience, New York, 1962.

[25]M. Suzuki and T. Oshima, "Estimation of the Coordination Number in a Multi-Component Mixture of Spheres," *Powder Technol.*, **35**, 159–66 (1983).

[26]R. F. Flatt, "Interparticle Forces and Superplasticizers in Cement Suspensions"; Ph.D. Thesis #2040, EPFL, 1999.

[27]Z. Zhou, "Rheology of Metal Oxide Suspensions"; Ph.D. Thesis, University of Melbourne, 2000.

[28]H-S Ma, A. P. Roberts, J.-H. Prévost, R. Jullien, and G. W. Scherer, "Mechanical Structure Property of Aerogels," *J. Non-Cryst. Solids*, **277**, 127–41 (2000).

[29]H. S. Ma, J.-H. Prévost, R. Jullien, and G. W. Scherer, "Computer Simulation of Mechanical Structure–Property Relationship of Aerogels," *J. Non-Cryst. Solids*, **285**, 216–21 (2001).

[30]F. de Larrard, *Concrete Mixture Proportioning*. E & FN Spon, London, 1999.

[31]R. J. Flatt, "Towards a Prediction of Superplasticized Concrete Rheology," *Mater. Struct.*, **27** [269] 289–300 (2004). □